Engineering Failure Analysis 51 (2015) 29–36

Contents lists available at ScienceDirect

Engineering Failure Analysis

journal homepage: www.elsevier.com/locate/engfailanal

Carburization of high-temperature steels: A simulation-based ranking of carburization resistance

G.F. Samaras, G.N. Haidemenopoulos *

Department of Mechanical Engineering, University of Thessaly, Pedion Areos, 38334 Volos, Greece

ARTICLE INFO

Article history:
Received 11 January 2015
Received in revised form 22 February 2015
Accepted 28 February 2015
Available online 9 March 2015

Keywords:
Carburization
Carbon profile
Carbide front
High temperature
API 530

ABSTRACT

Carburization is a failure mechanism affecting equipment, such as furnace tubes, operating at high temperatures. Carburization simulations were carried out for the heat-resistant steels referred to the API-530 standard by applying a model for carbon diffusion with the concurrent formation of alloy carbides. The calculated carbon and carbide volume fraction profiles were validated experimentally. The carburization layer is composed from $M_{23}C_6$ and M_7C_3 carbides. The time required for the carburization front to reach the mid-thickness of the tubes was used to characterize carburization resistance. The austenitic grades exhibit a higher carburization resistance than the ferritic grades at all temperatures. In the ferritic grades, alloy composition has a stronger effect at lower service temperatures (600 °C) where carburization resistance increases with Cr and Mo content. The acceleration of diffusion at high temperatures (800 °C) dominates the composition effects on carbon diffusion, and the carburization front is controlled by the formation of carbides, which in turn depends on the available amount of Cr in the steel. In the austenitic grades, the highest carburization resistance is exhibited by the stabilized grades 321 and 347 due to formation of TiC or NbC carbides respectively. Regarding the non-stabilized grades, carburization resistance is raised by addition of Mo (316 vs 304) and lower carbon (316L vs 316). The results of this study can be used for material selection for carburization resistance and for planning maintenance procedures for the timely replacement of tubes.

1. Introduction

Carburization is a high-temperature corrosion problem experienced in industrial processes such as ethylene production, natural gas reforming and coal gasification. The phenomenon takes place mainly in the petrochemical industry, where ethylene is produced in pyrolysis furnaces by thermal cracking of hydrocarbons in a steam hydrocarbon mixture at temperatures up to 1100 °C. In this cracking process, coke deposition occurs at the inner walls of the cracking tubes. In steam reformers natural gas or other hydrocarbons are converted by catalytic reaction on Ni-catalysts to CO and H_2 and carburization of tube walls is observed after over heating or excessive carbon activities. In industrial heat-treating furnaces for carburizing of steels, carburization of carrying grates and furnace walls is also observed. Components of the CO_2-cooled nuclear reactors may be carburized by CO_2, and the heat exchangers of helium reactors may be carburized by impurities such as CO and CH_4 in the helium gas. In coal gasification and in waste incineration plants carburization is possible, however sulfidation and corrosion by chlorine would be more severe processes [1,2]. Carburization takes place at high temperatures, and results

* Corresponding author.
E-mail addresses: gfsamaras@gmail.com (G.F. Samaras), hgreg@mie.uth.gr (G.N. Haidemenopoulos).

http://dx.doi.org/10.1016/j.engfailanal.2015.02.022
1350-6307/

in deterioration of Fe, Ni, and Co-base alloys. There are several damage processes caused by carburization, such as internal carbide formation in high-alloy steels in carbonaceous environments and metal dusting, a disintegration of metallic materials into a dust of graphite and metal particles in strongly carburizing atmospheres [3,4].

Carbon is transferred from the gas atmosphere through the porous coke at the alloy surface, where it diffuses in the interior and forms alloy carbides. Under most service conditions the materials are protected against carburization by an oxide layer, which serves as a barrier against carbon diffusion. The diffusion of carbon into the surface of a steel tube exposed to the combustion environment is enhanced by oxide-scale cracking and spallation and by operation at temperatures above the design specifications. The exposure of fresh metal to the carburizing environment enhances the carbon penetration. The oxide scale may crack or spall due to temperature changes during operation. In addition, a reducing atmosphere acts against the stability of the protective Cr_2O_3. There have been several experimental studies of carburization in the recent literature. Swaminathan et al. [5] studied the carburization failure of cast HK40+Nb alloy tubes of an air pre-heater unit in a petrochemical industry. The tubes failed prematurely after 13,000 h in service because of carburization attack from the flue gas on the inner wall side. Nawancy [6] examined pyrolysis furnace tubes made of HP45 heat-resistant steel casting to handle carbonaceous gases at about 850 °C in a petrochemical plant. These tubes developed longitudinal cracks after 22,000 h. Yin [7] studied the thermodynamics of carburization of 310 stainless steel exposed in carbon-rich CH_4/H_2 atmosphere for 500 h indicating that 1000 °C is an approximate limiting temperature, below which the environment exhibits a mixed oxidizing/carburizing behavior, while above this temperature a reducing/carburizing behavior is established. Kaya [8] investigated the carburization phenomenon in two tubular materials made from Fe–Cr–Ni-based HK40 alloy after a service life of approximately 25,000 h in an ethylene pyrolysis furnace. Catastrophic failures due to carburization of 9Cr–1Mo, 13CrMo44, 321H and TP304H steels were also reported in the literature for service life well below the design life [9–11]. Carburization failures due to extremely high temperatures have also been reported. Kaewkumsai et al. [12] reported a failure of an AISI 310 tube just one month after installation due to exposure to temperatures 200–250 °C above the design temperature. Hamid et al. [13] reported longitudinal cracks that in extreme cases penetrated the entire tube thickness. In this case the failure was due to a combination of creep and carburization attack because of exposure of the tube to an extremely high temperature. In addition to the experimental work, several theoretical works on carburization attack have been performed [1,8.15–17] mainly on the effect of alloy composition, carbon activity and temperature on the development of the carburization front.

Despite the theoretical and experimental work as well as the failure cases reported in the literature, carburization is not taken into account quantitatively in the design codes. For example, the API 530 standard used for the calculation of heater-tube thickness in petroleum refineries [14] provides guidelines for selection of tube materials based solely on criteria for creep resistance. Carburization is only mentioned as a potential mechanism that could limit the service life of the tubes. The aim of the present work is to provide a ranking of carburization resistance of the steels listed in the API 530 standard through a simulation of the carburization process. Simulations were performed by employing the computational kinetics software DICTRA [18], which can handle diffusion-controlled transformations, such as the alloy carbide formation during carbon diffusion. The carburization resistance was ranked according to the time required for the carburization front to reach the mid-thickness of the tubes. There are certain limitations under which the present model is applied. The first is related to the absence of a protective oxide layer at the surface. This situation is true when the oxide has spalled or under low partial oxygen pressure. Therefore, only carbon diffusion has been considered, without any oxygen diffusion and associated internal oxidation. The second limitation has to do with carbon activity at the surface. The carbon activity considered is established by the equilibrium of the steel surface with the gas phase. A carbon activity of 1 was applied as a boundary condition. This means that internal carbon deposition and metal dusting is not considered.

2. Methodology and calculations

A planar one-dimensional unit cell, depicted in Fig. 1 was employed for the simulations. The length L of the cell was taken equal to the thickness of the tube wall, 3 mm. The simulation was performed under the following assumptions:

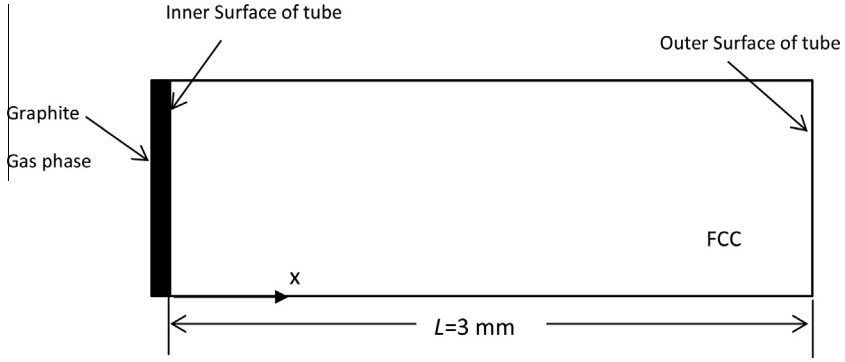

Fig. 1. Geometrical model showing the unit cell implemented for the carburization simulations. L is the thickness of the tube.

(a) Carbon is transferred from the gas atmosphere, through the porous coke, to the alloy surface.
(b) No oxide layer was considered in order to simulate carburization under low oxygen partial pressure or oxide spallation conditions.
(c) The temperature and concentration dependence of the diffusion coefficient of carbon was taken into account.
(d) Formation of alloy carbides was taken into account.

Under these assumptions, the concentration profile of the alloying elements in the x direction is described by the diffusion equation (Fick's 2nd law) as

$$\frac{\partial c_k}{\partial t} = -\frac{\partial J_k}{\partial x} \tag{1}$$

where c_k is the concentration and J_k is the diffusive flux of the component k.

The fluxes J_k are given by the Fick–Onsager law, for diffusion in multicomponent systems, which for n components takes the form

$$J_k = \sum_{j=1}^{n-1} D_{kj}^{n} \frac{\partial c_j}{\partial x} \tag{2}$$

where D_{kj}^{n} is the diffusion coefficient matrix, incorporated in DICTRA.

The boundary conditions at the left boundary (inner tube surface) are

$$a_C = 1 \tag{3}$$

$$\left.\frac{\partial c_k}{\partial x}\right|_{x=0} = 0 \quad \text{for } k \neq C \tag{4}$$

where a_C is the carbon activity. The system is closed (zero flux) for all elements except for carbon. At the right boundary (outer tube surface) the boundary conditions are

$$\left.\frac{\partial c_k}{\partial x}\right|_{x=L} = 0 \tag{5}$$

i.e. the system was considered to be closed for all elements.

For the solution of the diffusion Eq. (1) both thermodynamic and kinetic data are required. These data were retrieved from relevant thermodynamic and kinetic (mobility) databases. The diffusion coefficient in Eq. (2) was calculated by multiplying the respective mobilities with the relevant thermodynamic factor calculated by the Thermo-Calc computational thermodynamics software [19]. The thermodynamic database employed was the TCFE6 database for ferrous alloys, implemented in Thermo-Calc. The mobility database was the MOBFE2 database for ferrous alloys implemented in DICTRA. The initial composition of the steels used in the simulations is given in Table 1. These steels are listed in the API 530 standard and are used as tubing materials for high-temperature service. There are two group of steels in Table 1, ferritic Cr–Mo steels (P22, P21, P5, P9) and austenitic stainless steels (304, 316, 316L, 321, 347). Steels 321 and 347 are stabilized with Ti and Nb respectively. The phases considered for the simulation were the FCC austenite phase as the matrix phase and the alloy carbides $M_{23}C_6$, M_7C_3 and MC. These carbides were considered to precipitate during carburization in the austenitic matrix.

Table 1
Chemical composition (wt%) of the steels under evaluation according to API 530. Values in parentheses indicate the compositions used for the simulations.

Steel grade	C	Mn	Si	P	S	Cr	Ni	Mo	Ti	Nb
P22	0.05–0.15 (0.1)	0.3–0.6 (0.4)	0.5 max (0.4)	0.025	0.025	1.9–2.6 (2.25)	–	0.87–1.13 (1)	–	
P21	0.05–0.15 (0.1)	0.3–0.6 (0.4)	0.5max (0.4)	0.025	0.025	2.65–3.35 (3)	–	0.8–1.06 (1)	–	
P5	0.15max (0.1)	0.3–0.6 (0.4)	0.5max (0.4)	0.025	0.025	4–6 (5)	–	0.45–0.65 (0.5)	–	
P5b	0.15max (0.1)	0.3–0.6 (0.4)	1–2 (1.5)	0.025	0.025	4–6 (5)	–	0.45–0.65 (0.5)	–	
P9	0.15max (0.1)	0.3–0.6 (0.4)	0.25–1 (0.6)	0.025	0.025	8–10 (9)	–	0.9–1.1 (1)	–	
304	0.08	2	1max (0.8)	0.04max	0.03max	18–20 (18)	8–11 (10)	–	–	
316	0.08max (0.08)	2	0.75max (0.7)	0.04max	0.03max	16–18 (16)	8–11 (10)	2–3 (2)	–	
316L	0.035max (0.03)	2	0.75max (0.7)	0.04max	0.03max	16–18 (16)	10–15 (10)	2–3 (2)	–	
321	0.08max (0.08)	2	0.75max (0.7)	0.04max	0.03max	16–18 (16)	9–13 (10)	–	0.4–0.6 (0.5)	
347	0.08max (0.05)	2max (1)	0.75max (0.6)	0.04max	0.03max	17–20 (18)	9–13 (10)	–	–	1

3. Results and discussion

3.1. Experimental validation

Following Engstrom et al. [20], the methodology described above was validated with experimental data for a Ni–25Cr (wt%) alloy exposed at 850 °C for 1000 h in a carburizing atmosphere with a carbon activity $a_C = 1$.

The carbon profile established within the tube wall is shown in Fig. 2a. In the same diagram the experimental carbon profile determined by Bongartz et al. [21] is superimposed. A good agreement is exhibited between calculated and experimental values. In addition the profile of the volume fraction of the alloy carbides M_7C_3 and M_3C_2 is depicted in Fig. 2b, and is compared with the experimentally determined carbide distribution taken from Quadakkers et al. [22]. Again the agreement between calculated and experimental values is good. The presence of a 'discontinuity' of the carbon profile, in Fig. 2a, at about 0.5 mm is attributed to the transformation from M_7C_3 to M_3C_2 carbide with increasing carbon. This experimental validation allows the implementation of the methodology in carburization simulations of the steels listed in Table 1.

3.2. Representative calculations for 316 steel

Carburization simulations were carried out for all steels of Table 1. Representative calculations for the 316 austenitic stainless steel will be discussed in this section. The simulation was performed for a temperature of 800 °C. In Fig. 3a carbon concentration with distance from the inner surface of the tube is shown. The *x*-axis of the diagram corresponds to the tube wall thickness. The time required for the carburization front to reach a distance equal to half the thickness of the tube wall, termed carburization mid-thickness time $t_{1/2}$, is introduced to express the carburization resistance. From Fig. 3a it is depicted that the carbon profile reaches mid-thickness at a time of 222.2 h. At the same time, as depicted in Fig. 3b, the carbide front reaches mid-thickness. As carbon diffuses in the tube, it enriches the austenitic matrix and carbides are being formed in the carburized regions. Initially $M_{23}C_6$ (M = Cr, Fe) is formed, but as carbon concentration increases with time, the $M_{23}C_6$ is replaced by the M_7C_3 carbide. In addition to Quadakkers et al. [22], this transformation has been documented experimentally by Kaya [8].

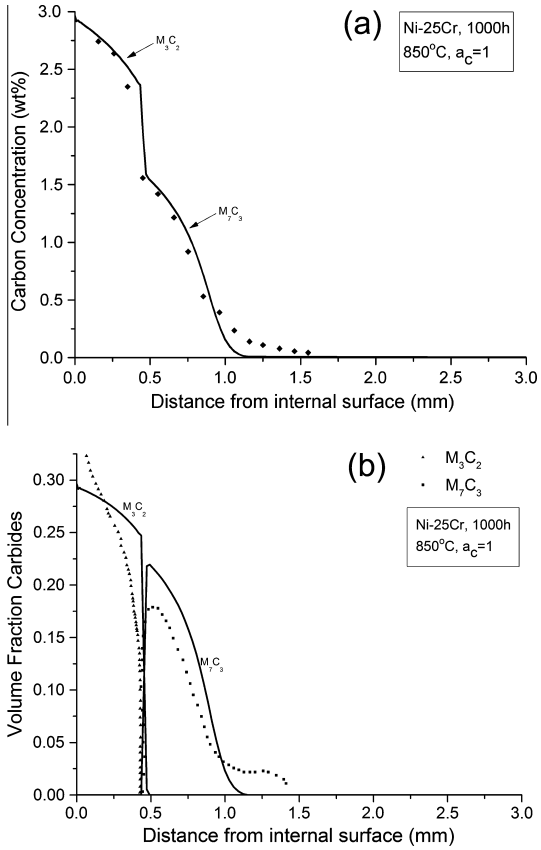

Fig. 2. (a) Comparison of calculated (solid line) and experimental (dotted line) [21] carbon concentration profile and (b) comparison of calculated (solid line) and experimental (dotted line) [22] carbide volume fraction profile for Ni–25Cr alloy exposed for 1000 h at 850 °C with unit carbon activity.

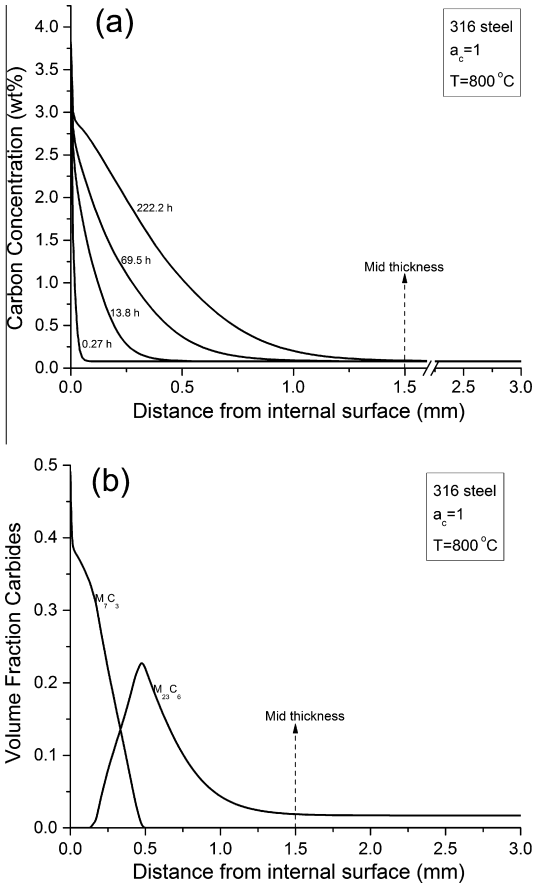

Fig. 3. Carburization simulation for 316 steel at 800 °C. (a) Evolution of carbon concentration profile with time. Carburization mid-thickness time is 222.2 h. (b) Profile of volume fraction carbides for 222.2 h carburization time.

It is also important to monitor chromium depletion from the austenite matrix in the carburized regions, since this affects the oxidation resistance of the tube material. The chromium profile in the tube wall for the mid-thickness time $t_{1/2}$ = 222.2 hours is shown in Fig. 4. The Cr depletion corresponds to 0.5 wt% Cr at the inner surface of the tube.

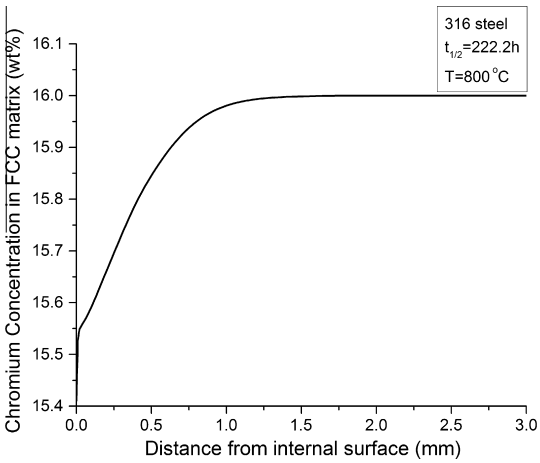

Fig. 4. Chromium profile for the carburization mid-thickness time of 222.2 h for 316 steel at 800 °C.

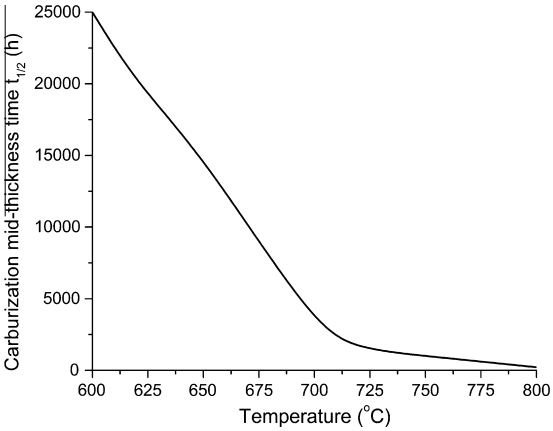

Fig. 5. Effect of temperature on the carburization mid-thickness time for 316 steel.

Temperature has a significant impact on carburization kinetics as demonstrated in Fig. 5, where calculations were performed for the temperature range 600–800 °C. The carburization mid-thickness time $t_{1/2}$ of tubes is reduced rapidly with temperature.

3.3. Ranking of carburization resistance

The calculated carburization mid-thickness time $t_{1/2}$ for the steels listed in Table 1 is depicted in Figs. 6 and 7 for service temperatures 600 and 800 °C respectively. The steels are grouped in two classes, ferritic and austenitic. The austenitic grades exhibit a much longer mid-thickness time than the ferritic grades at both temperatures. This behavior is attributed

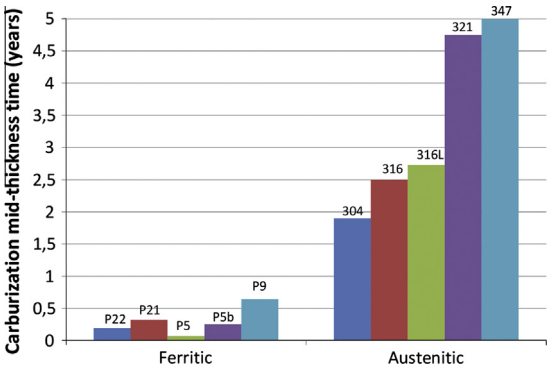

Fig. 6. Calculated carburization mid-thickness time, (3 mm tube thickness), for API 530 steels at 600 °C.

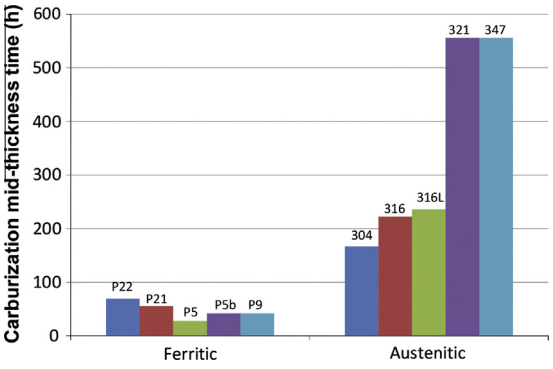

Fig. 7. Calculated carburization mid-thickness time, (3 mm tube thickness), for API 530 steels at 800 °C.

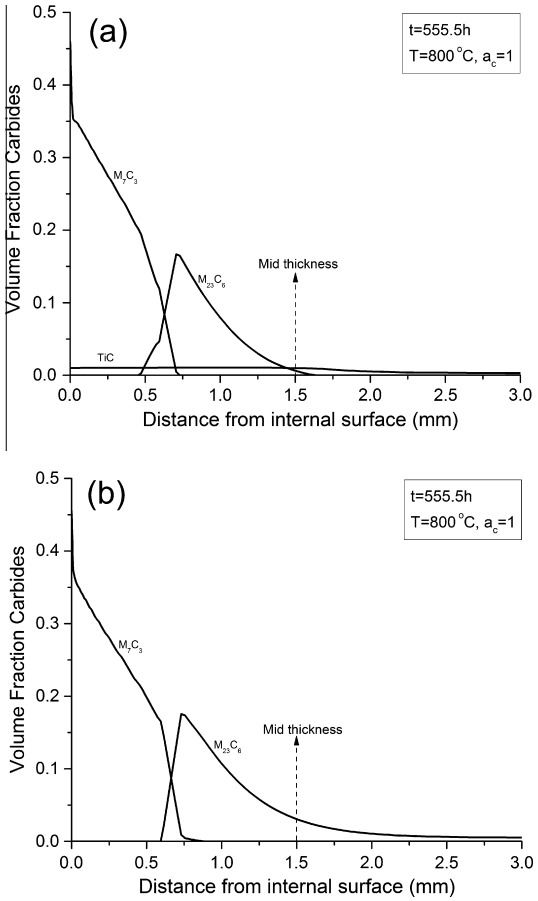

Fig. 8. Comparison of carbide volume fraction profiles for the carburization mid-thickness time of 555.5 h for 321 steel at 800 °C. (a) 321 steel and (b) 321 steel composition without Ti addition.

to the lower diffusion coefficient of carbon in the FCC matrix. The differences between the steels of the austenitic group are larger than those of the ferritic group. The ferritic steels exhibit more or less similar carburization resistance. Nevertheless some variations should be discussed. At 600 °C the P9 steel has the longest carburization mid-thickness time. This is attributed to the high Cr content, which in combination with the higher Mo content results in slower carbon diffusion. In addition the P5 steel exhibits the lowest carburization resistance due to the lower Mo content. The behavior is different at the higher temperature of 800 °C. The acceleration of diffusion at high temperature dominates the composition effects on carbon diffusion, and the carburization front is determined by the formation of carbides, which in turn depends on the available amount of Cr in the steel. Therefore, at 800 °C the P22 steel exhibits the longest carburization mid-thickness time among the ferritic steels. As discussed above the austenitic steels possess a much higher carburization resistance than the ferritic grades. Regarding the non-stabilized grades 304, 316 and 316L, carburization resistance is raised by addition of Mo (316 vs 304) and lower carbon (316L vs 316). The stabilized grades 321 and 347 exhibit the highest carburization resistance among the austenitic steels. This is attributed to the formation of MC carbides, preventing the diffusion of carbon at higher depth from the surface. In order to validate this observation a carburization simulation was carried out at 800 °C for the composition of steel 321 with and without addition of Ti. The results are shown in Fig. 8 where the carbide profiles are depicted for $t = 555.5$ h corresponding to the mid-thickness time for 321 steel. It is evident that for the steel without the Ti addition the carbide front goes beyond mid-thickness and reaches a much greater distance from the surface of the steel. There is a counter effect of MC carbides that requires attention. The interfaces between the MC carbides and the alloy matrix could provide a high diffusivity path and accelerate the diffusion of carbon in a way similar to that reported by Motin et al. [23] for the case of SiO_2 precipitates in Fe–Si alloys. However because of the low volume fraction of MC carbides this effect should be small.

The results presented above indicate that simulation of carburization could be a valuable tool in alloy selection for carburization resistance and for the development of suitable maintenance procedures for the timely replacement of tubes operating at high temperatures.

4. Conclusions

Carburization simulations were carried out for the heat-resistant steels referred to the API-530 standard by applying a model for carbon diffusion with the concurrent formation of alloy carbides. The method was validated experimentally. From the results presented above, the following conclusions can be drawn.

- The carburization layer is composed from $M_{23}C_6$ and M_7C_3 carbides. The M_7C_3 carbide is associated with higher carbon contents below the surface. In the Ti or Nb stabilized austenitic grades, MC carbides form, leading to improvement of the carburization resistance.
- The austenitic grades exhibit a higher carburization resistance than the ferritic grades at all temperatures.
- The ferritic grades exhibit similar carburization resistance. Alloy composition has a stronger effect at lower service temperatures (600 °C) where carburization resistance increases with Cr and Mo content. The acceleration of diffusion at high temperatures (800 °C) dominates the composition effects on carbon diffusion, and the carburization front is determined by the formation of carbides, which in turn depends on the available amount of Cr in the steel.
- In the austenitic grades, the highest carburization resistance is exhibited by the stabilized grades 321 and 347. Regarding the non-stabilized grades, carburization resistance is raised by addition of Mo (316 vs 304) and lower carbon (316L vs 316).

References

[1] Forseth S, Kofstad P. Metal dusting phenomenon during carburization of Fe–Ni–Cr alloys at 850–1000 °C. Mater Corros 1995;46:201–6.
[2] Matamala G, Canete P. Carburization of Fe–Ni–Cr Alloys in CH_4–H_2 Atmospheres between 900 and 1100 °C. Revista Latinoamericana de Metalurgia y Materiales 1998;8:67–72.
[3] Grabke HJ, Wolf I. Carburization and oxidation. Mater Sci Eng A 1987;87:23–33.
[4] Guttmann V, Burgel R. Effect of a carburizing environment on the creep behaviour of some austenitic steels. Corros Resist Mater Coal Convers Syst 1982:423–38.
[5] Swaminathan J, Singh R, Gunjan MR, Chattoraj I. Failure analysis of air pre-heater tubes of a petrochemicals plant. Eng Fail Anal 2009;16:2371–81.
[6] Tawancy HM. Degradation of mechanical strength of pyrolysis furnace tubes by high-temperature carburization in a petrochemical plant. Eng Fail Anal 2009;16:2171–8.
[7] Yin R. Carburization of 310 stainless steel exposed at 800–1100 °C in 2% CH_4/H_2 gas mixture. Corros Sci 2005;47. 1896-10.
[8] Kaya AA. Microstructure of HK40 alloy after high-temperature service in oxidizing/carburizing environment II. Carburization and carbide transformations. Mater Charact 2002;49:23–34.
[9] Ju GJ, Wu WZ, Dai SH. Failure of 9Cr–1Mo tubes in a feed furnace of dehydrogenation unit. Int J Press Vessel Pip 1997;74:199–204.
[10] Tanner GM. Metal dusting (catastrophic carburization) of a waste boil heat tube. Eng Fail Anal 1994;1:289–306.
[11] Lopez-Lopez D, Wong-Moreno A, Martinez L. Carburization processes involved in boiler-tube failures. Corros Sci 1993;35:1151–8.
[12] Kaewkumsai S, Khonraeng W, Sathirachinda N. High temperature failure of natural gas feed burner pipe. Eng Fail Anal 2013;27:74–83.
[13] Hamid AU, Tawancy HM, Mohammed ARI, Abbas NM. Failure analysis of furnace radiant tubes exposed to excessive temperature. Eng Fail Anal 2006;13:1005–21.
[14] API Standard 530. Calculation of heater tube thickness in petroleum refineries. 5th ed. American Petroleum Institute; 2003.
[15] Young DJ. Carburization and metal dusting. Shreir's Corros 2010;1:272–303.
[16] Li H, Zheng Y, Benum LW, Oballa M, Chen W. Carburization behaviour of Mn–Cr–O spinel in high temperature hydrocarbon cracking environment. Corros Sci 2009;51:2336–41.
[17] Matsukawa C, Hayashi S, Yakuwa H, Kishikawa T, Narita T, Ukai S. High-temperature carburization behaviour of HASTELLOY X in CH_4 gas. Corros Sci 2011;53:3131–8.
[18] Agren J. Computer simulations of diffusional reactions in complex steels. ISIJ Int 1992;32:291–6.
[19] Sundman B, Jansson B, Andersson JO. The thermo-calc databank system. CALPHAD 1985;9:153–90.
[20] Engstrom A, Hoglund L, Agren J. Computer simulation of diffusion in multicomponent systems. Metal Mater Trans A 1994;25A:1127–34.
[21] Bongartz K, Schulten R, Quadakkers WJ, Nickel H. Finite difference model describing carburization in high temperature alloys. Corrosion 1986;42:390–7.
[22] Quadakkers WJ, Schulten R, Bongartz K, Nickel H. A mathematical model describing carburization in multielement alloy systems. In: 10th int conf on metal corrosion, Madras, India; 1987.
[23] Motin MAA, Zhang J, Young DJ. Simultaneous corrosion of Fe–Si alloys by carbon and oxygen. J Electrochem Soc 2010;157:C375–81.